Multiple scattering in the Compton effect. II. Analytic and numerical treatment of energy profiles

Anthony C. Tanner and Irving R. Epstein*
Department of Chemistry, Brandeis University, Waltham, Massachusetts 02154
(Received 24 November 1975)

Energy profiles are calculated for photons scattered twice from stationary electrons in a cylindrical sample of infinite radius. Both double-Compton (inelastic) and one-Rayleigh (elastic), one-Compton events are treated. Klein-Nishina, Thomson, and isotropic differential cross sections are employed. It is found that at the energies typically used in γ-ray experiments, the different cross sections result in significantly different energy profiles and angular distributions, while at x-ray energies the form of the cross section is (as expected) considerably less important. Sample thickness and choice of primary scattering angle are found to have major effects on the shapes of the double-scattered profiles.

I. INTRODUCTION

Determination of the electron momentum distribution in matter by analysis of the spectrum of Compton-scattered radiation (the Compton profile) has become an increasingly important tool in chemistry and physics.[1] The analysis rests upon the fundamental equation

$$\frac{1}{E_1} = \frac{1}{E_0} + 2\sin^2\left(\frac{\theta}{2}\right) + \left(\frac{2}{E_0}\right)\left(\frac{p_z}{137}\right)\sin\left(\frac{\theta}{2}\right), \tag{1}$$

where E_0 and E_1 are the energies (in electron-rest-mass units) of the incident and scattered photons, respectively, θ is the angle of scattering, and p_z is the projection of the initial electron momentum (in atomic units) onto the scattering vector.

The validity of Eq. (1) is crucially dependent upon the assumption that each scattered photon interacts with only a single electron. Recently, it has become clear[2-5] that the electron momentum distribution inferred from a Compton profile may be significantly in error if the contribution of multiply-scattered photons to the observed spectrum is neglected.

In[6] Paper I of this series we posed two questions which must be answered if multiple scattering is to be accounted for. For a simplified model of a Compton experiment we were able to answer the first question, namely, to what extent are multiply-scattered photons being observed, by calculating analytically the angular distributions of single- and double-scattered photons. Here we present at least a partial solution to the second problem: how do multiply-scattered photons affect the observed energy spectrum?

Unfortunately, a completely analytic answer to this latter question does not appear possible, even within the model of Paper I. We do find, however, that the model of a cylindrical sample of very large radius (equivalent to an infinite-slab geometry) yields an expression for the energy profile which can be evaluated by a single numerical integration. We are thus able to obtain results using standard, accurate techniques for numerical integration rather than more elaborate and cumbersome multidimensional Monte Carlo procedures.[5,7,8] The Monte Carlo approach is, however, far easier to apply to models more general than the present one, and in[9] Paper III we use Monte Carlo calculations to investigate the effects of some of the approximations and assumptions made here.

Several previous investigators have undertaken analytic calculations of double-scattered energy spectra using various models and assumptions. Dumond[10] considered a spherical scatterer in which the first scattering is required to occur from a stationary electron at the center of the sphere. Williams *et al.*[4] extended this model to include both nonstationary electrons and elastic-inelastic double scattering events. By restricting the angle of observation to the value 90°, Kirkpatrick[11] was able to allow for first scatterings from noncentral electrons in a spherical sample and further to consider cylindrical samples, but only with central first scatterings. McIntire[12] has carried out a detailed analytic-numerical treatment of double scattering from all electrons in a cylindrical sample for the special case in which the scattered radiation is observed at 180° to the incident radiation, so that the entire scattering process occurs in a plane.

II. ENERGY PROFILES OF SINGLE-SCATTERED RADIATION

In an idealized model of a Compton scattering experiment, a monochromatic beam of photons of energy E_0 is scattered by stationary electrons, and only those photons singly scattered through the angle θ are observed. According to Eq. (1), under

such conditions the energy spectrum of scattered radiation will be a δ function centered at E_1.

In a real experiment, of course, no δ function is observed, since all the variables, and in particular the electronic momenta, assume a range of values, leading to a range of observed energies.

As an example, we calculate the energy spectrum of initially monochromatic radiation singly scattered by stationary electrons into a range of observation angles, θ_p. We assume the experimental geometry of Paper I: photons incident at right angles to a cylinder face of infinite radius and of optical thickness $\mu t = \omega$. We recall that $\partial P_1^\infty/\partial x$, where $x = \cos\theta$, is the angular distribution of the scattered photons, assuming no absorption, constant attenuation coefficient μ, and a classical (Thomson) differential scattering law. For stationary electrons, E_1 is given by

$$E_1(x) = \frac{E_0}{1 + E_0(1-x)}. \tag{2}$$

Then $[\partial P_1^\infty(\omega,x)/\partial x]\,dx$ is the probability of single scattering with $\cos\theta$ between x and $x + dx$, and $[\partial P_1^\infty(\omega,x(E))/\partial x]\,(\partial x/\partial E)dE$ is the probability of single scattering within a given energy range.

Thus the function $(\partial P_1^\infty/\partial x)\,(\partial x/\partial E)$ is the desired energy profile of scattered radiation, and we may write it using Eq. (2), with $E_1 \equiv E$, in the form

$$\frac{\partial P_1^\infty(\omega,E)}{\partial E} = \frac{1}{E^2}\,\frac{\partial P_1^\infty}{\partial x}, \tag{3}$$

where the analytic form of the angular distribution is given (for Thomson scattering) by[13]

$$\frac{\partial P_1^\infty(\omega,x)}{\partial x} = \tfrac{3}{8}(x^2+1)\,\frac{e^{\omega(1/x-1)}}{1/x-1} \times \begin{cases} e^{-\omega/x}, & 0 < x \leq 1 \\ 0, & x = 0 \\ 1, & -1 \leq x < 0. \end{cases}$$

Since $\partial P_1^\infty/\partial x$ is a function of sample thickness, it is clear that the energy profile $\partial P_1^\infty/\partial E$ will also vary with sample thickness. We can thus anticipate that the energy profile of double-scattered radiation will depend upon sample thickness as well. This variation has been observed by Williams and Halonen[14] in their Monte Carlo studies of double-scattered radiation, and it leads to fundamental difficulties[8] in applying straightforward extrapolation procedures to the problem of multiple scattering.

The variation of the single-scattered profile with sample thickness, *even if all other experimental parameters are held fixed,* has not previously been noted. It is not an artifact of our model, but a fundamental feature of a Compton-scattering experiment. This variation of the Compton profile with sample thickness is, however, *extremely small.* Even in our idealized model, the height at the peak of the profile changes by less than 1% as ω varies over two orders of magnitude. Inclusion of the effects of realistic momentum distributions, finite range of observation angles, instrumental resolution, etc., will tend to reduce the variation considerably, probably to the point where it is unobservable except perhaps by experiments specifically designed to detect it.

III. ENERGY PROFILES OF DOUBLE-SCATTERED RADIATION

A. Simple analytic example: Spherical-shell model

A nonmonochromatic scattered energy spectrum may be observed not only because the variables in Eq. (1) assume a range of values but also because of multiple scattering. We shall consider only the experimentally more important case of back-scattered radiation ($90° \leq \theta_p \leq 180°$), but the methods employed here are also applicable to forward scattering.

Consider a photon scattered first into a direction $\vec{k}_1$ defined by (θ_1, φ_1) and then into a direction $\vec{k}_2$ (θ_2, φ_2) with respect to $\vec{k}_1$. After the second scattering, the photon is observed in the laboratory frame to be traveling in a direction (θ_p, φ_p). If both scatterings are Compton, then the observed energy of the photon is obtained by two applications of Eq. (2):

$$E_2 = \frac{E_0}{1 + E_0(1 - \cos\theta_1 - \cos\theta_2)}. \tag{4a}$$

Of course, both scatterings need not be Compton. In general, we may describe an n-tuple scattering event by an ordered n-tuple $(i_1, i_2, \ldots, i_n)$, where $i_j = C$ for a Compton event and $i_j = R$ for a Rayleigh event. Equation (4a) thus describes a (C,C) event. For a (C,R) event

$$E_2 = \frac{E_0}{1 + E_0(1 - \cos\theta_1)}, \tag{4b}$$

while for a (R,C) event

$$E_2 = \frac{E_0}{1 + E_0(1 - \cos\theta_2)}. \tag{4c}$$

As discussed in Paper I, there are many sets of angles (θ_1, φ_1) and (θ_2, φ_2) through which a photon may double scatter and emerge with final direction (θ_p, φ_p) in the laboratory frame. The above equations (4) thus imply that a range of energies will be observed for double-scattered photons at any fixed angle θ_p.

We define the energy profile $I_{(C,C)}(E_2, \vec{k}_p)$ of double-Compton-scattered radiation as the probability density that a photon Compton scatters exactly twice and then exits in a direction $\vec{k}_p = (\theta_p, \varphi_p)$ with final energy E_2. Conservation of probability

(or photons) implies that

$$d\Omega_p \int_{E_{\min}}^{E_{\max}} dE_2\, I_{(C,C)}(E_2, \vec{k}_p) = \frac{\partial P_2}{\partial \Omega_p} d\Omega_p , \qquad (5)$$

where the upper and lower limits on E_2 are obtained in Appendix A. Equation (5) represents the total probability of observing double-Compton-scattered photons within $d\Omega_p$ of $\vec{k}_p$. In general, the energy profile will depend upon many more variables than those explicitly displayed in Eq. (5), e.g., attenuation coefficient, sample geometry, and initial photon energy, but for brevity we retain the notation of Eq. (5).

A particularly simple and instructive case of double scattering is that of scattering first from a single electron and then from a spherical shell of electrons centered on the first. The angular distribution for such a system is

$$\frac{\partial P_2}{\partial \Omega_p} = \int_0^{2\pi} d\varphi_1 \int_{-1}^{1} dx_1 \; \frac{d\sigma}{d\Omega_1} \; \frac{d\sigma}{d\Omega_2} . \qquad (6a)$$

Assuming Thomson scattering, we find as in Paper I

$$\frac{\partial P_2}{\partial \Omega_p} = \int_0^{2\pi} d\varphi_1 \int_{-1}^{1} dx_1 \frac{3}{16\pi}(x_1^2+1)\frac{3}{16\pi}(\cos^2\theta_2+1). \qquad (6b)$$

The integral of Eq. (6b) is evaluated explicitly in Ref. 13, but here we seek not the angular distribution, but the energy profile. We therefore make a change of variables from (x_1, φ_1) to (y, ϵ), where $y = x_1$, and $\epsilon = \cos\theta_1 + \cos\theta_2$. Note that for double-Compton scattering

$$E_2 = \frac{E_0}{1 + E_0(2-\epsilon)}. \qquad (7)$$

As shown in Appendix A, the above change of variables yields an integral of the form

$$\frac{\partial P_2}{\partial \Omega_p} = \int_{\epsilon_{\min}}^{\epsilon_{\max}} d\epsilon\, 2\left(\frac{3}{16\pi}\right)^2 \int_{y_l(\epsilon)}^{y_u(\epsilon)} \frac{P(y)}{[Q(y)]^{1/2}}. \qquad (8)$$

The forms of the polynomials $P(y)$ and $Q(y)$ are given and the integral (8) is calculated explicitly in Appendix A.

Applying the chain rule, we have

$$I_{(C,C)}(E, \vec{k}_p) = K_{(C,C)}(\epsilon, \vec{k}_p)\frac{\partial \epsilon}{\partial E_2} = \frac{1}{E_2^2} K_{(C,C)}(\epsilon, \vec{k}_p), \qquad (9)$$

where $K_{(C,C)}(\epsilon, \vec{k}_p)$ is the probability density for ϵ, i.e., the "ϵ profile." Conservation again yields an equation similar to Eq. (5):

$$\frac{\partial P_2}{\partial \Omega_p} d\Omega_p = d\Omega_p \int_{\epsilon_{\min}}^{\epsilon_{\max}} d\epsilon\, K_{(C,C)}(\epsilon, \vec{k}_p). \qquad (10)$$

The following identification of the ϵ profile follows directly from Eqs. (8) and (10):

$$K_{(C,C)}(\epsilon, \vec{k}_p) = 2\left(\frac{3}{16\pi}\right)^2 \int_{y_l(\epsilon)}^{y_u(\epsilon)} dy \frac{P(y)}{[Q(y)]^{1/2}}. \qquad (11)$$

Given an ϵ profile for some $\vec{k}_p$, the energy profile for any incident energy E_0 is easily obtained via Eqs. (4) and (9). Thus only a single ϵ profile is required for each $\vec{k}_p$. If E_2 is employed as the variable, a separate calculation of $I_{(C,C)}(E_2, \vec{k}_p)$ is necessary for each value of E_0. Thus use of the ϵ profile reduces the amount of computation considerably. This observation holds only if the integrand in Eq. (8) or Eq. (11) is independent of E_0, which condition holds for Thomson scattering.

Since (see Appendix A) the ϵ profile $K_{(C,C)}(\epsilon, \vec{k}_p)$ is independent of φ_p, we may integrate over φ_p to obtain $K_{C,C}(\epsilon, x_p)$, where as usual $x_p = \cos\theta_p$. When $\theta_p = 180°$, $K_{CC}(\epsilon, -1)$ is a δ function at $\epsilon = 0$. As the observation angle θ_p decreases toward 90°, $K_{CC}(\epsilon, x_p)$ flattens out and widens. This behavior is illustrated for several values of θ_p in Fig. 1(a), and is in good agreement with the trends noted by previous workers.[4,10] In Fig. 1(b) we show the ϵ profiles of once-elastic-, once-inelastic- scattered photons observed at the same θ_p. These K_{CR} (or K_{RC}) profiles are also calculated analytically in Appendix A. Note that these mixed profiles tend to be flatter and far less sensitive to choice of

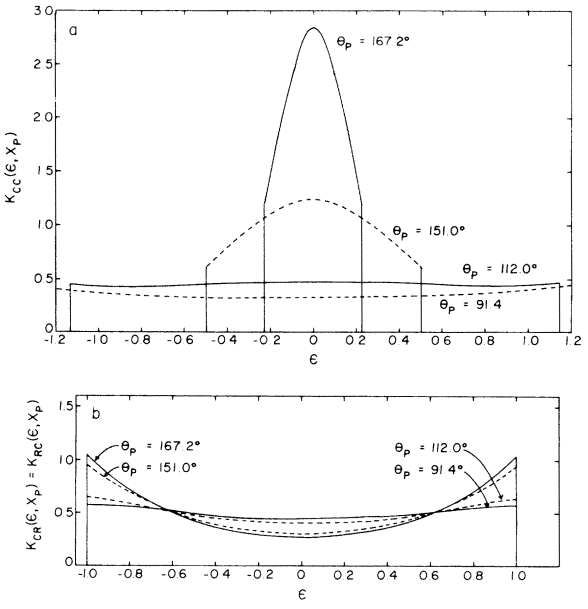

FIG. 1. ϵ profiles for double-scattered photons in the spherical-shell model. (a) Twice-Compton-scattered photons; (b) Once-Compton-, once-Rayleigh-scattered photons.

observation angle than the pure double-Compton profiles.

B. Infinite-radius-cylinder model

1. Thomson cross section; elastic and inelastic scattering

We now apply the method developed in Sec. III A to derive ϵ profiles for the sample geometry of Paper I, i.e., a cylinder of infinite radius. We again begin with the angular distribution of double-scattered radiation[6]:

$$\frac{\partial P_2^\infty}{\partial \Omega_p} = \int_0^\infty d\varphi_1 \int_{-1}^{1} dx_1 \frac{d\sigma}{d\Omega_1}\frac{d\sigma}{d\Omega_2} \times \int_0^\omega dv\, e^{-v} \int_0^{l_2} dl_2'\, \mu e^{-\mu l_2'} e^{-\mu l_3}. \tag{12}$$

Three distinct cases of double scattering now exist: (C,C), two successive Compton scatterings; (C,R), a Compton scattering followed by a Rayleigh scattering; (R,C), a Rayleigh scattering followed by a Compton scattering.

In each case we change variables to (ϵ, y), where ϵ is the sum of the cosines of the Compton scattering angles and for (C,C) scattering $y = x_1$, while for the mixed scatterings y is the cosine of the Rayleigh scattering angle. The ϵ profiles $K_{CC}(\epsilon, x_p)$, $K_{CR}(\epsilon, x_p)$, and $K_{RC}(\epsilon, x_p)$ are obtained by an integration over y:

$$K_{J_1J_2}(\epsilon, x_p) = \int_{y_l(\epsilon)}^{y_u(\epsilon)} dy\, F(y), \tag{13}$$

where $J_i = C$ or R. For generality we leave the exact form of the cross sections $(d\sigma/d\Omega_i)_{J_i}$, and hence of $F(y)$, unspecified for the moment.

This approach is quite general and may be extended to any order of scattering n, but with rapidly increasing difficulty as n increases. Unfortunately, the integration of Eq. (13) is, in general, not susceptible to analytic treatment as was Eq. (11). Numerical integration is therefore required. This introduces greater flexibility into the calculation, however, since numerical procedures can accomodate a large variety of integrands. Thus, as we shall see, variation of μ with energy of the scattered photon, as well as differential scattering laws more general than the Thomson cross section, may be taken into account. Explicit expressions for the three cases of Eq. (13) are derived in Appendix B.

The mixed profiles $K_{CR}(\epsilon, x_p)$ and $K_{RC}(\epsilon, x_p)$ are of interest because, unlike $K_{CC}(\epsilon, x_p)$, these double-scattered profiles do not approach the single-scattered profile in shape as θ_p approaches 180°.[4] Thus it will not be possible to eliminate the need for information about these profiles by going to very high scattering angles, as it may be for $K_{CC}(\epsilon, x_p)$. A rather surprising result emerges from our calculation. The profiles $K_{RC}(\epsilon, x_p)$ and $K_{CR}(\epsilon, x_p)$ *are not equivalent* for this geometry. For a spherical scatterer, the two profiles are equivalent, even for nonstationary electrons.[4]

In order to understand why (R,C) and (C,R) scattering are inequivalent in this model as well as to gain further insight into the shapes of the various profiles, we examine in detail a further simplification of our already simplified model. We consider a very thin sample ($\omega = 0.001$) and an observation angle θ_p with an isotropic scattering cross section for both Compton and Rayleigh scattering. We shall deal only with double-scattering sequences in a single plane, i.e., $\varphi_1 = 0$ in Eq. (A7) (φ_p has already been taken to be 0.) Under such conditions Eq. (A7) implies that if the first scattering angle is $\theta_1 \geq 180° - \theta_p$, then the second angle θ_2 may be either $\theta_p - \theta_1$ or $360° - (\theta_p + \theta_1)$. If $\theta_1 < 180° - \theta_p$, then the possibilities for θ_2 are $\theta_p \pm \theta_1$. The probability of scattering in such a thin sample is much less than 1 and varies little over the sample. Triple scattering will be essentially negligible.

We make the approximation that all photons which scatter have their first scattering at the center of the sample, $z = 0.0005$. The distance from this first scattering to the sample boundary is just (see Appendix A of Paper I)

$$l_{\theta_1} = 0.0005/|\cos\theta_1|$$

and the probability of scattering a second time before escaping is

$$P_2^{\theta_1} = 1 - e^{-l\theta_1} \tag{14}$$

The quantity $P_2^{\theta_1}$ gives, within this crude model, the profile of double-scattered radiation, where the appropriate value of ϵ will be determined by whether the sequence of scatterings is (C,C), (R,C), or (C,R). We note that $P_2^{\theta_1}$ reaches a maximum value of 1 when $\theta_1 = 90°$. That is, a photon scattered first through 90° *must* double scatter because of the finite-radius geometry. We therefore expect peaks in our double-scattered energy profiles corresponding to events for which $\theta_1 = 90°$. For (C,R) scattering, $\epsilon = \cos\theta_1$ and we expect a peak at $\epsilon = 0$. For (C,C) scattering $\epsilon = \cos\theta_1 + \cos\theta_2$ and we expect peaks at $\epsilon = \cos\theta_2 = \cos(\theta_p - 90°)$ and at $\cos(270° - \theta_p)$. For (R,C) scattering, $\epsilon = \cos\theta_2$, and the peaks should fall at the same ϵ values as the (C,C) peaks. With $\theta_p = 167°$, these peaks should lie at $\cos 77°$ and $\cos 103°$ or at $\epsilon = \pm 0.225$, while at $\theta_p = 100°$, the values are $\epsilon = \pm 0.984$.

The normalized profiles shown in Figs. 2–5

illustrate this behavior. The locations of the peaks agree with the above analysis far better than might have been anticipated, though, of course, the simple analysis becomes increasingly inadequate as ω increases, since the probability of scattering is no longer constant throughout the sample, and because triple scattering becomes significant.

We now consider the inequivalence of the (C, R) and (R, C) profiles in a bit more detail. It is clear that for ϵ sufficiently close to zero, we

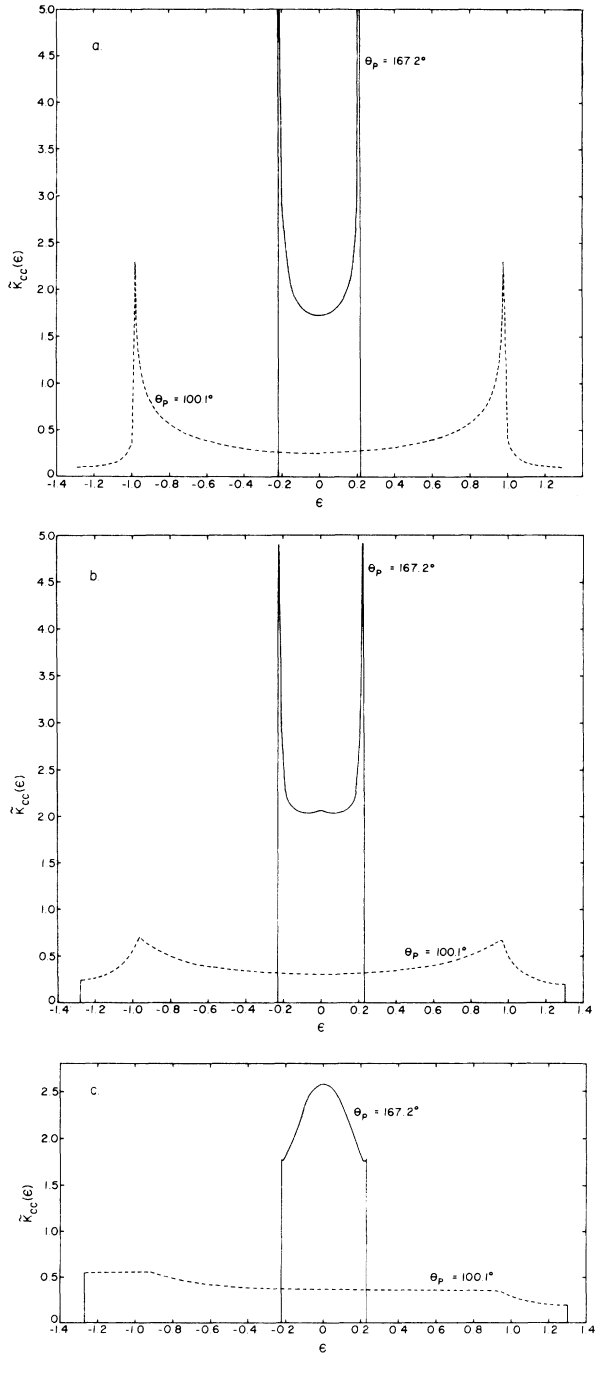

FIG. 2. Normalized ϵ profiles for double-Compton scattering. Profiles are normalized so that $\int_{\epsilon_{min}}^{\epsilon_{max}} \tilde{K}_{CC}(\epsilon, x_p)\, d\epsilon = 1$. (a) $\omega = 0.001$; (b) $\omega = 0.1$; (c) $\omega = 5.0$. Profiles change very little for $\omega > 5.0$.

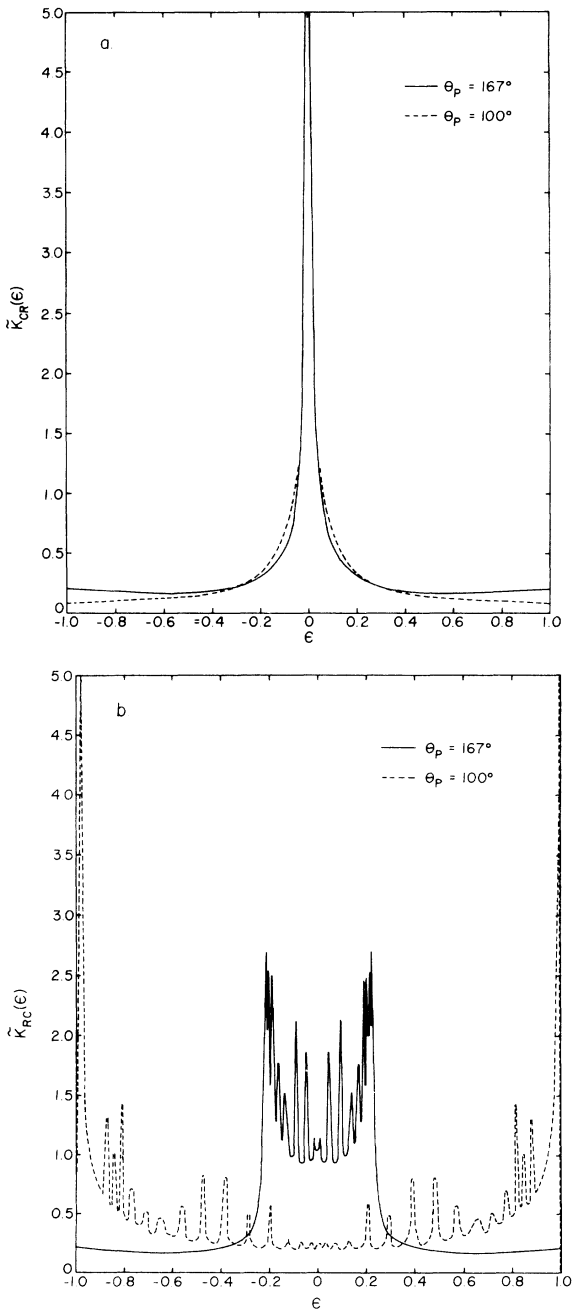

FIG. 3. Normalized ϵ profiles for mixed double scattering with $\omega = 0.001$. (a) Compton-Rayleigh; (b) Rayleigh-Compton.

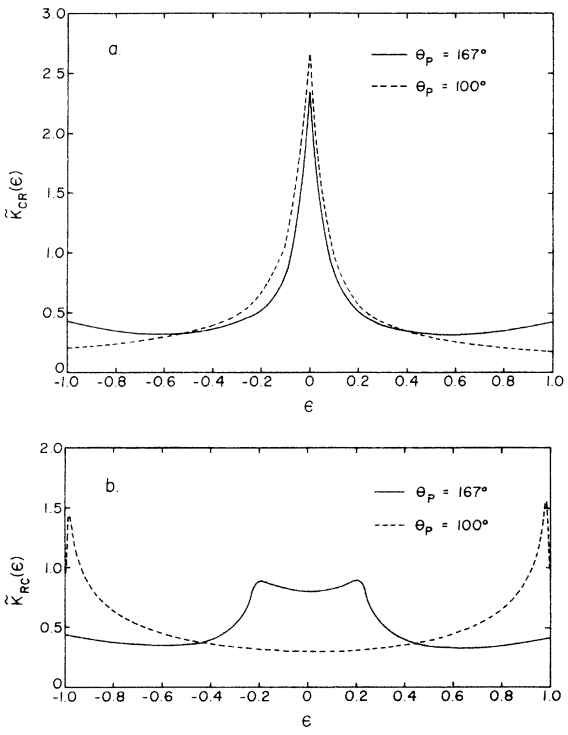

FIG. 4. Normalized ϵ profiles for mixed double scattering with $\omega = 0.1$. (a) Compton-Rayleigh; (b) Rayleigh-Compton.

must have

$$K_{CR}(\epsilon, x_p) > K_{RC}(\epsilon, x_p), \quad \epsilon \sim 0, \tag{15}$$

since such scatterings correspond to a Compton-scattering angle near 90°, and hence to the peaks in the (C, R) profile as discussed above. We note

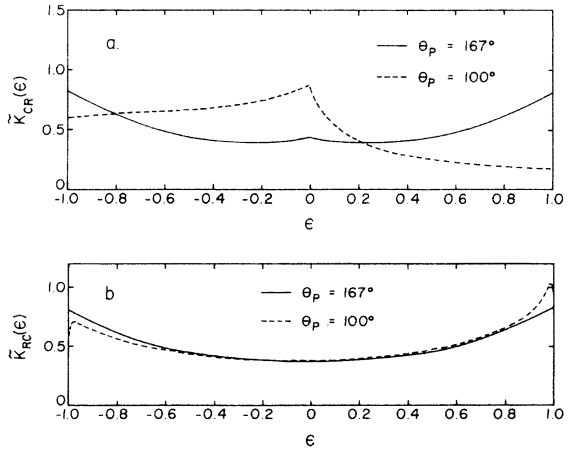

FIG. 5. Normalized ϵ profiles for mixed double scattering from thick samples ($\omega = 5.0$). (a) Compton-Rayleigh; (b) Rayleigh-Compton.

that since $\epsilon = \cos\theta_1$ and $P_2^{\theta_1}$ depends only upon $\cos\theta_1$ [via Eq. (14)] $K_{CR}(\epsilon, x_p)$ must be symmetric about $\epsilon = 0$. Also, since our scattering cross sections are identical for Compton or Rayleigh scattering if we neglect coherent scattering, the angular distributions $(\partial P_2^{\infty}/\partial\Omega_p)_{J_1 J_2}$ must be the same for all (J_1, J_2), since the integrand in Eq. (12) is the same for all (J_1, J_2). Equation (10) applied to the three types of double scattering then implies that there must be some critical values of $|\epsilon|$, ϵ_C, beyond which the inequality (15) is reversed, since the integrals over the entire ϵ profile must be equal. If we examine the double-scattering events shown in Fig. 6, we see that the probability of (C, R) scattering with $\epsilon = \cos 10°$ is

$$2P_2^{10°} = 1.015 \times 10^{-3}.$$

By symmetry, (C, R) scattering at 170° has the same probability. For (R, C) scattering with $\epsilon = \cos 10°$ we have

$$P_2^{157°} + P_2^{177°} = 1.044 \times 10^{-3},$$

and at $\epsilon = \cos 170°$, the probability is

$$P_2^{3°} + P_2^{23°} = 1.044 \times 10^{-3}.$$

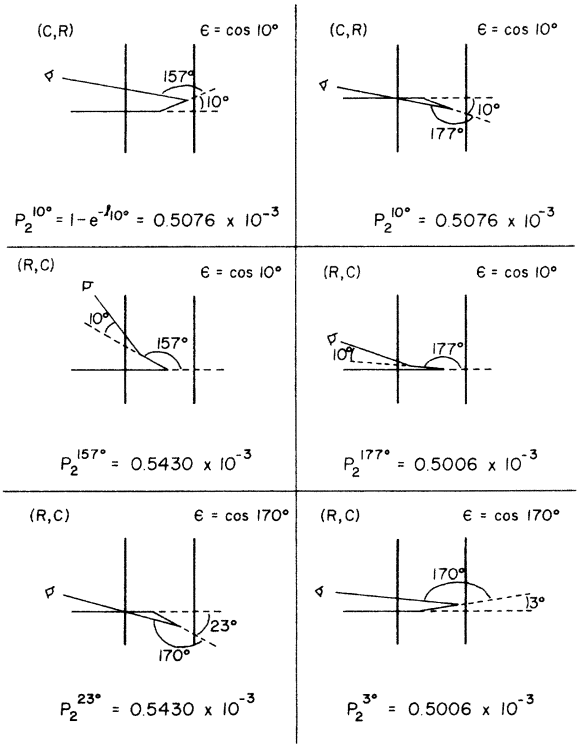

FIG. 6. Planar double scattering events with $\theta_p = 167°$, $|\epsilon| = \cos 10° = 0.9848$.

A similar analysis applied to any other set of angles reveals that (a) the (R, C) profile is symmetric about $\epsilon = 0$ in this approximation, and (b) for $|\epsilon| > \epsilon_C$ we have

$$K_{RC}(\epsilon, x_p) > K_{CR}(\epsilon, x_p),$$

i.e., there are two and only two points where the (C, R) and (R, C) profiles cross. Also, the value of ϵ_C may be expected to increase with increasing ω, as the region around 90° where a second scattering becomes highly probable widens with increasing ω.

The true situation is, of course, considerably more complex than the simple case discussed here, since the actual cross sections are not isotropic and since the overwhelming majority of scattering events will be nonplanar. The somewhat surprising oscillations in the (R, C) profiles seen in Fig. 3 presumably result from these factors. The figures show that in all cases asymmetries about $\epsilon = 0$ are enhanced with increasing ω. Finally, the drastic changes in the shapes of the double-scattered profile as we vary the sample thickness do not bode well for simple extrapolation procedures.

We note that many of the more striking features noted above, such as oscillations, sharp peaks, and asymmetries in the double-scattered profiles are exaggerated by our model. In actual experiments such effects should be less noticeable because (a) photons will be observed over a range of scattering angles, so the actual observed profile $K_{J_1 J_2}$ will be an integral of the form

$$K_{J_1 J_2}(\epsilon) = \int dx_p \, K_{J_1 J_2}(\epsilon, x_p);$$

(b) photoelectric absorption will compete with the scattering processes; and (c) a finite-radius cylinder will eliminate the certainty of a second scattering at 90°, thus making maxima resulting from 90° initial scatterings less sharp.

We recall, however, as noted in Paper I (and as will be shown numerically in Paper III), that actual samples with high attenuation coefficients are often "effectively infinite" in radius. The effects of photoelectric absorption on the energy profiles will be examined later in this paper, when we consider the variation of μ with energy.

Finally, we note that as θ_p decreases, $K_{CC}(\epsilon, x_p)$ becomes relatively flat, and the interval $(\epsilon_{\min}, \epsilon_{\max})$ increases in width. $K_{RC}(\epsilon, x_p)$ always extends from $\epsilon = -1$ to $\epsilon = 1$, but the oscillations become less intense and the profile in general flattens, except around $|\epsilon| = 1$. On the other hand, the single-scattered profile (for moving electrons) narrows as θ_p decreases. One rough method of correcting for multiple scattering in experiments might be to measure Compton profiles at relatively small angles and treat double-scattered (and possibly all multiply-scattered) radiation as a flat background, especially if the probability of elastic scattering is low, since then K_{CR} (and K_{RC}) would be small. If desired, one could then remeasure the profile at a higher angle to obtain better resolution and use the low-angle data together with the theoretical angular dependence of double scattering[6] to make the correction.

2. *Other differential cross sections*

In Appendix B, we derive expressions for the ϵ profiles for general differential cross section $d\sigma/d\Omega$ with the only restriction being that $d\sigma/d\Omega$ be symmetric about $\varphi = 0$.[15] In this section we shall compare $\tilde{K}_{CC}(\epsilon, x_p)$ for isotropic and Klein-Nishina cross sections with the corresponding ϵ profiles calculated using the Thomson cross section. We treat only double-Compton scattering since the Klein-Nishina differential cross section

$$\left(\frac{d\sigma}{d\Omega}\right) = \frac{r_0^2}{2}\left(\frac{E_1}{E_0}\right)^2\left(\frac{E_1}{E_0} + \frac{E_0}{E_1} - \sin^2\theta\right) \tag{16}$$

reduces to the Thomson expression for elastic scattering, for which $E_1 = E_0$:

$$\left(\frac{d\sigma}{d\Omega}\right)_{\text{Th}} = \frac{r_0^2}{2}(1 + \cos^2\theta). \tag{17}$$

Thus any differences between (R, C) or (C, R) Klein-Nishina profiles and the corresponding Thomson profiles will be smaller then differences between the (C, C) profiles calculated with the two different scattering laws.

In addition to differences in the normalized ϵ profiles $\tilde{K}_{CC}(\epsilon, x_p)$ for the various cross sections, we must also consider the question of the absolute ϵ profiles $K_{CC}(\epsilon, x_p)$. Since

$$\int_{\epsilon_{\min}}^{\epsilon_{\max}} d\epsilon \, K_{CC}(\epsilon, x_p) = \frac{\partial P_2}{\partial x_p}, \tag{18}$$

while for $\tilde{K}_{CC}(\epsilon, x_p)$ the integral gives unity, the differences between absolute ϵ profiles may easily be obtained from the normalized profiles and the angular distributions $\partial P_2/\partial x_p$ which are given in Table I. This problem has already been treated analytically in Paper I for the isotropic differential cross section

$$\left(\frac{d\sigma}{d\Omega}\right)_{\text{is}} = \frac{1}{4\pi}.$$

As a check on our numerical integration procedure, both the analytic results of Paper I and the numerical results obtained by integrating the absolute ϵ profiles are given for the isotropic and Thomson cases.

TABLE I. Angular distribution $\partial P_2^{\infty}/\partial x_p$ for double Compton scattering.

Method	ω	$\theta_p = 100°$ 0.001	1.0	5.0	$\theta_p = 167°$ 0.001	1.0	5.0
Isotropic [a]		0.204×10^{-5}	0.3620×10^{-1}	0.3822×10^{-1}	0.195×10^{-5}	0.1244	0.1704
Isotropic [b]		0.195×10^{-5}	0.3623×10^{-1}	0.3824×10^{-1}	0.193×10^{-5}	0.1244	0.1704
Thomson [a]		0.1686×10^{-5}	0.3405×10^{-1}	0.3615×10^{-1}	0.1293×10^{-5}	0.1144	0.1643
Thomson [b]		0.1689×10^{-5}	0.3405×10^{-1}	0.3618×10^{-1}	0.1280×10^{-5}	0.1144	0.1643
Klein-Nishina ($E_0 = 0.0174$ MeV) [b,c]		0.1711×10^{-5}	0.3373×10^{-1}	0.3576×10^{-1}	0.1322×10^{-5}	0.1142	0.1639
Klein-Nishina ($E_0 = 0.0595$ MeV) [b,d]		0.1700×10^{-5}	0.3294×10^{-1}	0.3485×10^{-1}	0.1299×10^{-5}	0.1122	0.1611
Klein-Nishina ($E_0 = 0.159$ MeV) [b,e]		0.1636×10^{-5}	0.3135×10^{-1}	0.3297×10^{-1}	0.1181×10^{-5}	0.1058	0.1519

[a] Calculated analytically as in Paper I (Ref. 6).
[b] Obtained by numerical integration of $K_{CC}(\epsilon, x_p)$.
[c] Mo $K\alpha$ x rays.
[d] Am γ rays.
[e] Te γ rays.

In Fig. 7, we compare normalized ϵ profiles calculated from the Thomson cross section with those from the Klein-Nishina cross section at incident energies corresponding to the standard x-ray and γ-ray sources. Use of the Klein-Nishina formula appears to make little difference for x-rays and, somewhat surprisingly, the high-angle γ-ray profile is quite similar in shape to that given by the Thomson cross section. At smaller angles the differences become more marked. Table I suggests that the absolute profiles will differ somewhat more than the normalized profiles of Fig. 7.

In Paper I it was concluded that differences between normalized angular distributions calculated using different differential cross sections decrease with increasing ω. This does not appear to be the case for energy profiles. The difference between the Thomson and the Klein-Nishina profiles for either Mo $K\alpha$ or Am radiation does decrease with sample thickness. However, the opposite behavior is observed in comparing the Thomson and isotropic profiles, while the difference between Thomson and Te γ-ray ϵ profiles appears to almost independent of ω.

3. *Variation of attenuation coefficient with photon energy*

In Appendix B we define f_i as the probability that a photon-electron interaction is of the ith type, where $i = C$ for Compton scattering, R for Rayleigh scattering, and τ for photoelectric absorption. We have

$$f_i = \mu_i / \mu,$$

where $\mu = \mu_C + \mu_R + \mu_\tau$. Photoelectric absorption is thus accounted for in the f_i factors.

One method of treating this photoelectric absorption in (C, C) scattering, for example, is simply to assume constant values for the μ_i's and then to multiply the values of $(\partial P_2^{\infty}/\partial \Omega_p)_{CC}$ and $K_{CC}(\epsilon, x_p)$ by f_C^2.

Since, however, the μ_i and hence the f_i vary with energy, the above approach may be a rather crude approximation. Profiles $K_{CC}(\epsilon, x_p)$ for water were therefore calculated in the following manner, which takes into account the variation of μ with

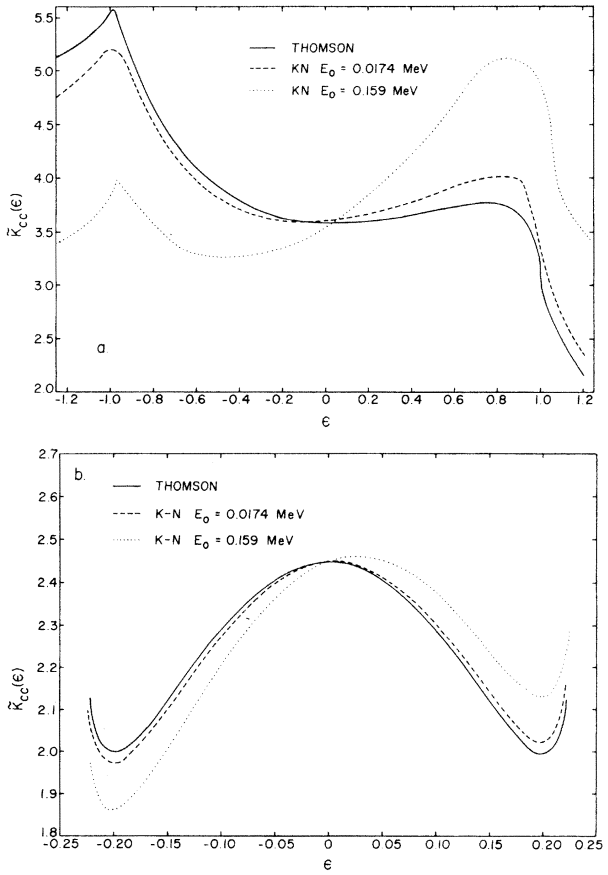

FIG. 7. Normalized ϵ profiles for double-Compton scattering with $\omega = 1.0$. (a) $\theta_p = 100°$; (b) $\theta_p = 167°$.

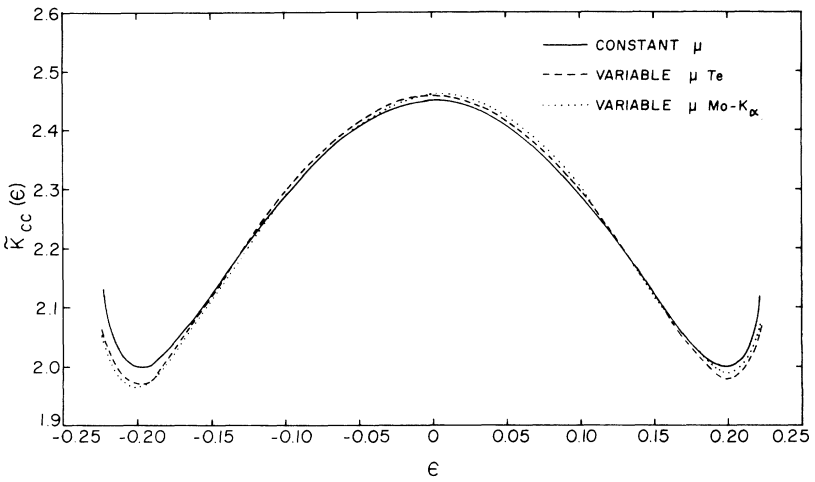

FIG. 8. Effect of variable attenuation coefficients on normalized ϵ profiles for double-Compton scattering from water with $\omega = 1.0$ and $\theta_p = 167°$.

energy: Tabulated values[16] of the μ_i were graphed and values of μ and μ_c were compiled from the tabulations or, if necessary, from the graphs for energies ranging from 0.005 to 0.160 MeV in 0.005-MeV increments. The numerical integration (see Appendix B) to give $K_{CC}(\epsilon, x_p)$ was then carried out using a program which linearly interpolated to obtain the values of μ and μ_c at energies between those for which μ and μ_c were stored.

As Fig. 8 shows, for either Mo $K\alpha$ or Te radiation, the normalized profile, i.e., the shape of the double-Compton-scattered spectrum, is changed very little by the inclusion of variable attenuation coefficients. Angular distributions and hence absolute (C, C) profiles appear to be affected somewhat more than normalized profiles. It appears that neglect of the variation of μ with energy may introduce errors of about 10% in $(\partial P_2/\partial \Omega_p)$ for x-ray photons and about 4% for γ rays. In Table II we compare some ϵ profiles and angular distributions calculated with and without allowance for the variation of μ. Note that since μ decreases with energy in the region of interest, the absolute profile calculated by allowing μ to vary will always lie below the absolute profile obtained under the simpler assumption that μ is constant at the value corresponding to the incident radiation. The difference is roughly twice as large for x rays as for γ rays. Note also that the asymmetry of the ϵ profile is enhanced by the variation of μ, again much more so for the lower-energy photons.

IV. SUMMARY AND CONCLUSIONS

Defining a variable ϵ as the sum of the sum of the cosines of the Compton-scattering angles, we have derived a method for calculating ϵ profiles for any primary scattering angle greater than 90°

TABLE II. Absolute ϵ profiles and angular distributions for double-Compton scattering from water with $\omega = 1.0$, $\theta_p = 167°$.

	$E_0 = 0.0174$ MeV (Mo $K\alpha$)		$E_0 = 0.159$ MeV (Te)	
ϵ	$10^2 \times f_c^2 K_{CC}(\epsilon, x_p)$ Fixed μ	$10^2 \times K_{CC}(\epsilon, x_p)$ Variable μ	$f_c^2 K_{CC}(\epsilon, x_p)$ Fixed μ	$K_{CC}(\epsilon, x_p)$ Variable μ
−0.200	0.4844	0.4303	0.2195	0.2084
−0.140	0.5234	0.4705	0.2371	0.2273
−0.100	0.5548	0.5010	0.2513	0.2417
−0.039	0.5872	0.5323	0.2660	0.2565
0.000	0.5934	0.5386	0.2688	0.2594
0.039	0.5872	0.5335	0.2660	0.2568
0.100	0.5548	0.5039	0.2513	0.2425
0.140	0.5232	0.4743	0.2370	0.2280
0.200	0.4840	0.4349	0.2193	0.2089
$\left(\frac{\partial P_2^\infty}{\partial x_p}\right)^a$	0.2425	0.2190	0.1099	0.1058

[a] Calculated by numerical integration of the absolute ϵ profile.

for three possible sequences of double scattering from stationary electrons in a cylinder of infinite radius. Double-scattered energy profiles can easily be obtained from these ϵ profiles. The scattering sequences treated are two Compton scatterings (C,C), a Compton followed by a Rayleigh scattering (C,R), and finally Rayleigh-Compton (R,C) scattering. The latter two cases have been found to be quite different for the sample geometry used here, though the difference is not experimentally observable.

For (C,C) scattering, the ϵ profiles were first calculated using the Thomson differential cross section and a constant attenuation coefficient. Variation of either the primary scattering angle θ_p or the sample thickness resulted in sizable changes in both the shapes and magnitudes of the profiles.

The use of cross sections other than the Thomson was also studied. At the low energies used in Compton x-ray experiments, differences resulting from use of the Klein-Nishina expression are small, as expected, but for high-energy Te γ-ray photons these differences become significant.

Calculations which allowed for photoelectric absorption and the variation of attenuation coefficient with energy of the scattered photon showed that the latter effect is considerably greater for 0.017-MeV x rays than for 0.159-MeV γ rays.

ACKNOWLEDGMENT

Acknowledgment is made to the donors of the Petroleum Research Fund, administered by the American Chemical Society, for support of this research.

APPENDIX A: DOUBLE SCATTERING IN THE SPHERICAL-SHELL MODEL

We derive here ϵ profiles for radiation scattered first by a single electron and then again by a spherical shell of electrons centered on the first. We begin with a somewhat more general form of Eq. (6a):

$$\frac{\partial P_2}{\partial \Omega_p} = \int_0^{2\pi} d\varphi_1 \int_{-1}^{1} dx_1 \left(\frac{d\sigma}{d\Omega_1}\right)_I \left(\frac{d\sigma}{d\Omega_2}\right)_J , \tag{A1}$$

where I and J may be either C or R depending upon whether the scattering is elastic or inelastic. Only Thomson scattering is considered here, so that

$$\left(\frac{d\sigma}{d\Omega_i}\right)_C = \frac{3}{16\pi}(\cos^2\theta_i + 1), \tag{A2}$$

while for elastic scattering (including coherent scattering at small angles),

$$\left(\frac{d\sigma}{d\Omega_i}\right)_R = \frac{1}{n_R}(\cos^2\theta_i + 1) \times \begin{cases} 1 & \text{if } -1 \leq \cos\theta_i \leq \cos\theta_c \\ Z & \text{if } \cos\theta_c \leq \cos\theta_i \leq 0, \end{cases} \tag{A3}$$

where Z is the atomic number of the scatterer, $\theta_c = Z^{1/3}/E(\text{keV})$, and n_R is the normalization constant:

$$n_R = 2\pi[\tfrac{4}{3}(Z+1) + (x_c^3/3 + x_c)(1-Z)], \tag{A4}$$

where $x_c = \cos\theta_c$.

For the cross sections considered here, the integrand in (A1) is symmetric about $\varphi_1 = \pi$, and thus

$$\frac{\partial P_2}{\partial \Omega_p} = 2\int_0^{\pi}\int_{-1} dx \left(\frac{d\sigma}{d\Omega_1}\right)_I \left(\frac{d\sigma}{d\Omega_2}\right)_J . \tag{A5}$$

From Paper I, we have

$$\cos\theta_2 = \sin\theta_p \sin\theta_1 \cos(\varphi_p - \varphi_1) + \cos\theta_p \cos\theta_1 . \tag{A6}$$

Since the problem also possesses symmetry about the polar (cylinder) axis, $\partial P_2/\partial\Omega_p$ is independent of φ_p, which for convenience we set equal to zero in (A6) to obtain

$$\cos\theta_2 = \sin\theta_1 \sin\theta_p \cos\varphi_1 + \cos\theta_p \cos\theta_1 . \tag{A7}$$

A change of variable, from (x_1, φ_1) to (y, ϵ) is made for the three cases of (C,C), (C,R), and (R,C) scattering.

Case I: (C,C) scattering. For this case we let $\epsilon = \cos\theta_1 + \cos\theta_2$ and $y = x_1$. Then

$$\varphi_1 = \cos^{-1}\left(\frac{\epsilon - y(1+x_p)}{(1-x_p^2)^{1/2}(1-y^2)^{1/2}}\right). \tag{A8}$$

The Jacobian for this transformation is

$$\frac{\partial(x_1,\varphi_1)}{\partial(y,\epsilon)} = \frac{\partial\varphi_1}{\partial\epsilon} = \frac{-1}{(1-\cos^2\varphi_1)^{1/2}} \frac{\partial\cos\varphi_1}{\partial\epsilon} . \tag{A9}$$

The region of integration in Eq. (A5) is $\{(x_1,\varphi_1): -1 \leq x_1 \leq 1;\ 0 \leq \varphi \leq \pi\}$. Figure 9 is the image of that region in the (y,ϵ) plane when $\cos\theta_p = -0.9$. Note that for a given ϵ, y may range from some lower value y_l to some upper value y_u, both of which are functions of ϵ. For a given x_p, the upper and lower limits on ϵ are obtained by letting φ_1 vary from 0 to π. Thus the boundary in Fig. 9 corresponds to points in the (x_1,φ_1) plane with $\varphi_1 = 0$ or π, or with $x_1 = \pm 1$. Note that for boundary points with $\varphi_1 = 0$ or π, $\cos^2\varphi_1 = 1$ and the Jacobian, Eq. (A9), becomes infinite. This Jacobian expressed in terms of ϵ, y, and x_p explicitly is

$$\left|\frac{\partial(x_1,\varphi)}{\partial(y,\epsilon)}\right| = \frac{1}{[Q(y)]^{1/2}},$$

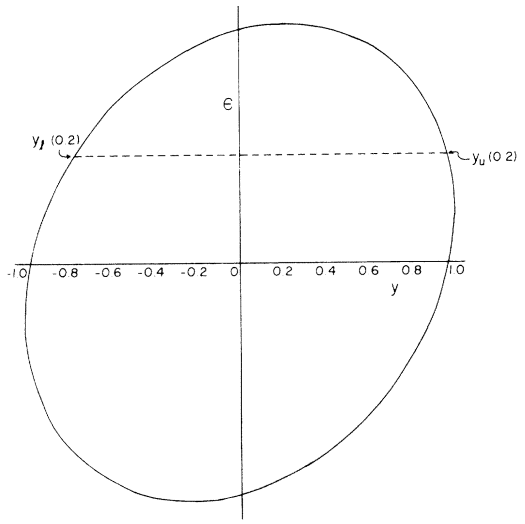

FIG. 9. Region of integration in the (y,ϵ) plane when $\cos\theta_p = -0.9$.

where

$$Q(y) = -2(1+x_p)y^2 + 2\epsilon(1+x_p)y + 1 - \epsilon^2 - x_p^2 \tag{A10}$$

is a quadratic in y whose coefficients depend upon ϵ and x_p. Since y_u and y_l are on the boundary of Fig. 9, they correspond to points for which $(1-\cos^2\varphi_1)^{1/2}=0$, i.e., the roots of $Q(y)$:

$$\begin{aligned} y_u(\epsilon) &= \tfrac{1}{2}\{\epsilon + [\epsilon^2 + 2(1-x_p^2-\epsilon^2)/(1+x_p)]^{1/2}\}, \\ y_l(\epsilon) &= \tfrac{1}{2}\{\epsilon - [\epsilon^2 + 2(1-x_p^2-\epsilon^2)/(1+x_p)]^{1/2}\}. \end{aligned} \tag{A11}$$

Making the transformation of variables from (A5), we obtain

$$\frac{\partial P_2}{\partial \Omega_p} = \int_{\epsilon_{\min}}^{\epsilon_{\max}} \int_{y_l(\epsilon)}^{y_u(\epsilon)} dy \, \frac{(d\sigma/d\Omega_1)_c (d\sigma/d\Omega_2)_c}{[Q(y)]^{1/2}} .$$

Assuming Thomson scattering, we let

$$P(y) = \left(\frac{d\sigma}{d\Omega_1}\right)_c \left(\frac{d\sigma}{d\Omega_2}\right)_c .$$

Identifying y with x_1 and using Eq. (A7) yields

$$P(y) = (3/16\pi)^2[y^4 - 26y^3 + (\epsilon^2+2)y^2 + 2\epsilon y + 1 + \epsilon^2]. \tag{A12}$$

$P(y)$ is thus a polynomial in y whose coefficients depend only on ϵ. The upper and lower limits $\epsilon_{\min}$ and $\epsilon_{\max}$ occur when the two roots of $Q(y)$, $y_u(\epsilon)$ and $y_l(\epsilon)$, coincide. Thus, setting the terms in Eq. (A11) equal we have $\epsilon_{\max} = -\epsilon_{\min} = [2(1+x_p)]^{1/2}$.

As in Eq. (11), we identify the ϵ profile

$$\begin{aligned} K_{(C,C)}(\epsilon, \vec{k}_p) &= 2\int_{y_l(\epsilon)}^{y_u(\epsilon)} dy \, \frac{(d\sigma/d\Omega_1)_c (d\sigma/d\Omega_2)_c}{[Q(y)]^{1/2}} \\ &= 2\int_{y_l(\epsilon)}^{y_u(\epsilon)} dy \, \frac{P(y)}{[Q(y)]^{1/2}} \end{aligned}$$

or

$$K_{(C,C)}(\epsilon, \vec{k}_p) = 2\left(\frac{3}{16\pi}\right)^2 \sum_{n=0}^{4} C_n \int_{y_l(\epsilon)}^{y_u(\epsilon)} dy \, \frac{y^n}{[Q(y)]^{1/2}} ,$$

where the C_n are the coefficients of y^n in $P(y)$, Eq. (A12).

We define the auxiliary functions

$$H_n(z_1, z_2, a, b, c) \equiv \int_{z_1}^{z_2} dx \, \frac{x^n}{[p(x)]^{1/2}} , \tag{A13}$$

where $p(x) = ax^2 + bx + c$ is a quadratic in x. These functions are evaluated explicitly in Appendix C for a specific class of quadratics $p(x)$.

The results of Appendix C show that

$$K_{(C,C)}(\epsilon, \vec{k}_p) = 2\left(\frac{3}{16\pi}\right)^2 \sum_{n=0}^{4} C_n \bar{H}_n(a,b,c), \tag{A14}$$

where

$$\bar{H}_n(a,b,c) \equiv H_n(y_l, y_u, a_Q, b_Q, c_Q), \tag{A15}$$

and y_l and y_u are the roots [Eq. (A11)] and a_Q, b_Q, and c_Q the coefficients (A10) of the polynomial $Q(y)$. Note that both the coefficients C_n and the arguments of the H_n are functions of ϵ.

Case II: *(C,R) scattering.* For this case, let

$$\epsilon = x_1 \quad \text{with } -1 \le \epsilon \le 1,$$

$$y = x_2 \quad \text{with } y_l(\epsilon) \le y \le y_u(\epsilon).$$

Then

$$\varphi_1 = \cos^{-1}\left(\frac{y - \epsilon x_p}{(1-x_p^2)^{1/2}(1-\epsilon^2)^{1/2}}\right).$$

The Jacobian for this transformation is

$$\frac{\partial(x_1, \varphi_1)}{\partial(y, \epsilon)} = \frac{\partial \varphi_1}{\partial y} = \frac{-1}{[R(y)]^{1/2}} , \tag{A16}$$

where, like $Q(y)$, $R(y)$ is a quadratic in y whose coefficients depend upon ϵ and x_p:

$$R(y) = -y^2 + 2\epsilon x_p y + 1 - \epsilon^2 - x_p^2. \tag{A17}$$

The roots of $R(y)$ are

$$\begin{aligned} y_u(\epsilon) &= \epsilon x_p + (1-x_p^2)^{1/2}(1-\epsilon^2)^{1/2}, \\ y_l(\epsilon) &= \epsilon x_p - (1-x_p^2)^{1/2}(1-\epsilon^2)^{1/2}. \end{aligned}$$

Proceeding as in the (C,C) case, we have

$$\frac{\partial P_2}{\partial \Omega_p} = 2\int_{-1}^{1} d\epsilon \, (d\sigma/d\Omega_1)_C \int_{y_l(\epsilon)}^{y_u(\epsilon)} \frac{(d\sigma/d\Omega_2)_R}{[R(y)]^{1/2}} , \tag{A18}$$

where the cross sections $(d\sigma/d\Omega_i)_I$ are given by

Eqs. (A2) and (A3). Noting that the Compton cross section is independent of y, we again identify the ϵ profile:

$$K_{(C,R)}(\epsilon,\vec{k}_p)=2\left(\frac{d\sigma}{d\Omega_1}\right)_C\int_{y_l(\epsilon)}^{y_u(\epsilon)}dx\,\frac{(d\sigma/d\Omega_2)_R}{[R(y)]}\,. \tag{A19}$$

Utilizing the analogs of Eqs. (A13) and (A15), we obtain

$$K_{(C,R)}(\epsilon,\vec{k}_p)=2\left(\frac{3}{16\pi}\right)(\epsilon^2+1)\frac{1}{n_R}\times\begin{cases}\bar{H}_2(a_R,b_R,c_R)+\bar{H}_0(a_R,b_R,c_R), & \text{if } y_u(\epsilon)\le y_c\\ Z[H_2(y_u(\epsilon),y_c,a_R,b_R,c_R)+H_0(y_u(\epsilon),y_c,a_R,b_R,c_R)]\\ \quad+H_2(y_c,y_l(\epsilon),a_R,b_R,c_R)+H_0(y_c,y_l(\epsilon),a_R,b_R,c_R), & \text{if } y_c<y_u(\epsilon).\end{cases} \tag{A20}$$

Case III: (R,C) scattering. For this case, let

$\epsilon=x_2$ with $-1\le\epsilon\le1$,

$y=x_1$ with $y_l(\epsilon)\le y\le y_u(\epsilon)$.

Then

$$\varphi_1=\cos^{-1}\left(\frac{\epsilon-yx_p}{(1-x_p^2)^{1/2}(1-y^2)^{1/2}}\right)$$

and the Jacobian is

$$\frac{\partial(x_1,\varphi_1)}{\partial(y,\epsilon)}=\frac{\partial\varphi_1}{\partial\epsilon}=\frac{-1}{[R(y)]^{1/2}}\,,$$

with $R(y)$ as in Eq. (A17) and $y_u(\epsilon)$ and $y_l(\epsilon)$ the roots of $R(y)$.

Proceeding in a by now familiar manner, we have

$$\frac{\partial P_2}{\partial\Omega_p}=2\int_{-1}^{1}d\epsilon\left(\frac{d\sigma}{d\Omega_2}\right)_C\int_{y_l(\epsilon)}^{y_u(\epsilon)}\frac{(d\sigma/d\Omega_1)_R}{[R(y)]^{1/2}} \tag{A21}$$

which is equivalent to Eq. (A18). Thus

$$K_{(R,C)}(\epsilon,\vec{k}_p)=2\left(\frac{d\sigma}{d\Omega_2}\right)_C\int_{y_l(\epsilon)}^{y_u(\epsilon)}dy\,\frac{(d\sigma/d\Omega_1)_R}{R(y)}, \tag{A22}$$

which on substitution of the cross sections is seen to be identical to Eq. (A19), so that in this case

$$K_{(R,C)}(\epsilon,\vec{k}_p)=K_{(C,R)}(\epsilon,\vec{k}_p).$$

APPENDIX B: DOUBLE SCATTERING IN THE INFINITE-CYLINDER MODEL

We treat here a slightly more general model of scattering from an infinite-radius cylinder than employed in Paper I. In order to allow for inclusion of processes other than Compton scattering, cross sections other than Thomson, and the variation of attenuation coefficient with energy, we adopt a modified notation: μ_i is the attenuation coefficient between the ith and $(i+1)$th scatterings; l_i' is the distance between the ith and $(i+1)$th scatterings; l_i is the distance between ith scattering and the cylinder boundary along the direction of motion of the scattered photon; f_{I_i} is the probability that the $(i+1)$th scattering will be of type I; $(d\sigma/d\Omega)_{J_i}$ is the Jth type of differential scattering cross section (normalized to 1) for the ith scattering, a function of $\cos\theta_i$ (but not of φ_i), E_{i-1}, and E_i.

We recall that μ_i is a function of E_i, the photon energy after the ith scattering, which itself depends upon E_{i-1} and the ith scattering angle, via Eq. (1). Since

$$f_{I_i}=\mu_{I_i}\Big/\sum_I\mu_{I_i},$$

the f_{I_i} are also functions of the E_i.

The angular distribution of double-scattered photons for the above model is defined analogously to Eq. (D1) of Ref. 13:

$$\frac{\partial P_2^\infty}{\partial\Omega_p}=\int_0^{l_0}dl_0'\,\mu_0e^{-\mu_0l_0'}f_0\times\int_0^{2\pi}d\varphi_1\int_{-1}^{1}dx_1\left(\frac{d\sigma}{d\Omega_1}\right)_{J_1}\times\int_0^{l_1}dl_1'\,\mu_1e^{-\mu_1l_1'}f_1\left(\frac{d\sigma}{d\Omega_2}\right)_{J_2}e^{-\mu_2l_2},$$

where $l_0=t$ for cylindrical samples. Interchanging the order of integration and recalling the symmetry about $\varphi_1=0$, we have

$$\frac{\partial P_2^\infty}{\partial\Omega_p}=2f_0\int_0^{\pi}d\varphi_1\int_{-1}^{1}dx_1f_1\left(\frac{d\sigma}{d\Omega_1}\right)_{J_1}\left(\frac{d\sigma}{d\Omega_2}\right)_{J_2}\times L(t,\vec{k}_1,\vec{k}_p,\mu_0,\mu_1,\mu_2), \tag{B1}$$

where the geometry-dependent terms have been grouped together as

$$L(t,\vec{k}_1,\vec{k}_p,\mu_0,\mu_1,\mu_2)\equiv\int_0^{l_0}dl_0'\,\mu_0 e^{-\mu_0 l_0'}\int_0^{l_1}dl_1'\,\mu_1 e^{-\mu_1 l_1'} e^{-\mu_2 l_2}.$$

The relations of Paper I give

$$L(t,\vec{k}_1,\vec{k}_p,\mu_0,\mu_1,\mu_2)=\frac{\mu_0\mu_1}{(\mu_1-\mu_2 x_1/x_p)}\times\begin{cases}\dfrac{1-e^{-(\mu_0-\mu_2/x_p)t}}{\mu_0-\mu_2/x_p}-\dfrac{1-e^{-(\mu_0-\mu_1/x_p)t}}{\mu_0-\mu_1/x_1} & \text{if } -1\le x_1\le 0\\ \dfrac{1-e^{-(\mu_0-\mu_2/x_p)t}}{\mu_0-\mu_2/x_p}+\dfrac{e^{-(\mu_0-\mu_2/x_p)t}-e^{-(\mu_1/x_1-\mu_2/x_p)t}}{\mu_0-\mu_1/x_1} & \text{if } 0\le x_1\le 1.\end{cases}\quad\text{(B2)}$$

Whenever the denominator of some term in Eq. (B2) is zero, the function assumes the form 0/0. Straightforward application of l'Hopital's rule then shows that the function L is uniformly continuous. It should be noted, however, that L is not smooth at $x_1=0$.

The angular distribution (B1) is similar in form to those of Appendix A; the new features are the exponential attenuation terms in the function $L(t,\vec{k}_1,\vec{k}_p,\mu_0,\mu_1,\mu_2)$ and the energy-dependent terms [e.g., f_i, μ_i, and in some cases $(d\sigma/d\Omega_i)$]. The same changes of variable as in Appendix A will yield the ϵ profiles. However, because of the energy-dependent terms in the integrand of the transformed integral, the y integration must, in general, be performed numerically.

With the above remarks and reference to the results of Appendix A, the expressions for the ϵ profiles are now easily derived.

Case I: (C, C) scattering.

$$K_{(C\,C)}(\epsilon,\vec{k}_p)=2f_0\int_{y_l(\epsilon)}^{y_u(\epsilon)}dy\,f_1\frac{(d\sigma/d\Omega_1)_C(d\sigma/d\Omega_2)_C}{[Q(y)]^{1/2}}\times L(t,\vec{k}_1,\vec{k}_p,\mu_0,\mu_1,\mu_2),\quad\text{(B3)}$$

with

$$-[2(1+x_p)]^{1/2}\le\epsilon\le[2(1+x_p)]^{1/2}\quad\text{(B4a)}$$

and

$$y_u(\epsilon)=\epsilon+[\epsilon^2+2(1-x_p^2-\epsilon^2)/(1+x_p)]^{1/2},\quad\text{(B4b)}$$

$$y_l(\epsilon)=\epsilon-[\epsilon^2+2(1-x_p^2-\epsilon^2)/(1x_p)]^{1/2}.\quad\text{(B4c)}$$

$Q(y)$ is given by Eq. (A10) and from Eq. (A7), the cosine of the second scattering angle is

$$x_2=(1-y^2)^{1/2}(1-x_p^2)^{1/2}\cos\varphi+yx_p.$$

Since y_u and y_l are the roots of $Q(y)$, the integrand diverges at the limits of integration and for the actual numerical quadrature we therefore change variable to

$$z_Q=\frac{2(-a_Q)^{1/2}}{\pi}\int\frac{dy}{[Q(y)]^{1/2}}=\frac{-2}{\pi}\sin^{-1}\left(\frac{3a_Q+b_Q}{(b_Q^2-4a_Qc_Q)^{1/2}}\right).\quad\text{(B5)}$$

After some algebra, Eq. (B3) takes the form

$$K_{(C,C)}(\epsilon,\vec{k}_p)=\frac{f_0\pi}{(-a_Q)^{1/2}}\int_{-1}^{1}dz_Q f_1\left(\frac{d\sigma}{d\Omega_1}\right)_C\left(\frac{d\sigma}{d\Omega_2}\right)_C\times L(t,\vec{k}_1,\vec{k}_p,\mu_0,\mu_1,\mu_2).\quad\text{(B6)}$$

Case II: (C, R) scattering. In this case we have

$$K_{(C,R)}(\epsilon,\vec{k}_p)=2f_0\left(\frac{d\sigma}{d\Omega_1}\right)_C\times\int_{y_l(\epsilon)}^{y_u(\epsilon)}dx\,\frac{f_1(d\sigma/d\Omega_2)_R L(t,\vec{k}_1,\vec{k}_p,\mu_0,\mu_1,\mu_2)}{[R(y)]^{1/2}},$$

with

$$-1\le\epsilon\le1$$

and

$$y_u(\epsilon)=\epsilon x_p+(1-x_p^2)^{1/2}(1-\epsilon^2)^{1/2},$$

$$y_l(\epsilon)=\epsilon x_p-(1-x_p^2)^{1/2}(1-\epsilon^2)^{1/2}.$$

$R(y)$ is given by Eq. (A17), and since we have made the transformation $y=x_2$, the function $L(t,\vec{k}_1,\vec{k}_p,\mu_0,\mu_1,\mu_2)$ defined in Eqs. (B1) and (B2) is independent of y and may be taken outside the integral. We make a change of variable analogous to Eq. (B5),

$$z_R=\frac{2(-a_R)^{1/2}}{\pi}\int\frac{dy}{[R(y)]^{1/2}}=\frac{-2}{\pi}\sin^{-1}\left(\frac{2a_R y+b_R}{(b_R^2-4a_Rc_R)^{1/2}}\right)\quad\text{(B7)}$$

and finally obtain

$$K_{(C,R)}(\epsilon,\vec{k}_p)=\frac{\pi}{(-a_R)^{1/2}}f_0\left(\frac{d\sigma}{d\Omega_1}\right)_C\times L(t,\vec{k}_1,\vec{k}_p,\mu_0,\mu_1,\mu_2)\int_{-1}^{1}dz_R\,f_1\left(\frac{d\sigma}{d\Omega}\right)_R.\quad\text{(B8)}$$

Case III: (R, C) *scattering*. Now

$$K_{(R,C)}(\epsilon, \vec{k}_p) = 2f_0\left(\frac{d\sigma}{d\Omega_2}\right)_C \times \int_{y_l(\epsilon)}^{y_u(\epsilon)} dy \frac{(d\sigma/d\Omega_1)_R L(t, \vec{k}_1, \vec{k}_p, \mu_0, \mu_1, \mu_2)}{[R(y)]^{1/2}} \tag{B9}$$

or, with the change of variable of Eq. (B7)

$$K_{(R,C)}(\epsilon, \vec{k}_p) = \frac{\pi}{(-a_R)^{1/2}} f_0\left(\frac{d\sigma}{d\Omega_2}\right)_C \times \int_{-1}^{1} dz_R f_1\left(\frac{d\sigma}{d\Omega_1}\right)_R L(t, \vec{k}_1, \vec{k}_p, \mu_0, \mu_1, \mu_2) \tag{B10}$$

Since all the ϵ profiles are independent of φ_p, we may define

$$K_{J_1 J_2}(\epsilon, x_p) \equiv 2\pi K_{(J_1, J_2)}(\epsilon, \vec{k}_p).$$

The function L in the integrands of Eqs. (B6) and (B9) is not smooth at $y = 0$. These points correspond to the values $z_0 = z_Q(0)$ and $z_R(0)$ in Eqs. (B5) and (B7), respectively. In the actual calculations, each point in the ϵ profile for $x_p = \cos\theta_p$ was evaluated using a 48-point Gauss-Legendre quadrature from -1 to z_0, another 48-point quadrature from z_0 to 1, and then summing the two portions. These ϵ profiles were integrated over all allowed ϵ using n 20-point Gauss-Legendre grids to yield the value of the angular distribution at x_p. The value of n required to obtain good agreement with the analytical Thomson angular distributions of Paper I varied from 1 for $\omega \gtrsim 0.5$ to 10 for $0.001 \lesssim \omega \lesssim 0.05$.

APPENDIX C: FUNCTIONS $\mathcal{H}_n$, H_n, AND $\bar{H}_n$

Consider a polynomial

$$p(x) = ax^2 + bx + c.$$

We wish to evaluate integrals of the form

$$H_n(z_1, z_2, a, b, c) = \int_{z_1}^{z_2} dx \frac{x^n}{[p(x)]^{1/2}}$$

for $n = 0, 1, 2, 3, 4$.

Define

$$\mathcal{H}_m(x, a, b, c) = \int dx \frac{x^m}{[p(x)]^{1/2}}.$$

Reference 17 gives the indefinite integral

$$\int dx \frac{x^m}{[p(x)]^{(2J+1)/2}} = \frac{x^{m-1}}{(m-2J)a[p(x)]^{(2J-1)/2}} - \frac{(2m-2J-1)b}{2(m-2J)a} \int dx \frac{x^{m-1}}{[p(x)]^{(2J+1)/2}} - \frac{(m-1)c}{(m-2J)a} \int dx \frac{x^{m-2}}{[p(x)]^{(2J+1)/2}}.$$

Thus for $m = 4$, $J = 0$, we have

$$\mathcal{H}_4(x, a, b, c) = \int dx \frac{x^4}{[p(x)]^{1/2}} = \frac{x^3}{4a}[p(x)]^{1/2} - \frac{7b}{8a} \int dx \frac{x^3}{[p(x)]^{1/2}} - \frac{3c}{4a} \int dx \frac{x^2}{[p(x)]^{1/2}},$$

so that

$$\mathcal{H}_4(x, a, b, c) = \frac{x^3}{4a}[p(x)]^{1/2} - \frac{7b}{8a}\mathcal{H}_3(x, a, b, c) - \frac{3c}{4a}\mathcal{H}_2(x, a, b, c).$$

Reference 17 also gives

$$\mathcal{H}_3(x,a,b,c) = \left(\frac{x^3}{3a} - \frac{5bx}{12a^2} + \frac{5b^2}{8a^3} - \frac{2c}{3a^2}\right)[p(x)]^{1/2} - \left(\frac{5b^3}{16a^3} - \frac{3bc}{4a^2}\right)\mathcal{H}_0(x, a, b, c),$$

$$\mathcal{H}_2(x,a,b,c) = \left(\frac{x}{2a} - \frac{3b}{4a^2}\right)[p(x)]^{1/2} + \left(\frac{3b^2}{8a^2} - \frac{c}{2a}\right)\mathcal{H}_0(x, a, b, c),$$

$$\mathcal{H}_1(x,a,b,c) = \frac{1}{a}[p(x)]^{1/2} - \frac{b}{2a}\mathcal{H}_0(x, a, b, c).$$

For the polynomials $Q(x)$ and $R(x)$ of Appendixes A and B it can be shown that (i) $a < 0$; (ii) $b^2 > 4ac$; (iii) $|2ax + b| < (b^2 - 4ac)^{1/2}$. Then from Ref. 18,

$$\mathcal{H}_0(x,a,b,c) = \frac{-1}{(-a)^{1/2}} \sin^{-1}\left(\frac{2ax+b}{(b^2-4ac)^{1/2}}\right).$$

The definite integrals H_n are now defined as

$$H_n(z_1, z_2, a, b, c) \equiv \int_{z_1}^{z_2} dx \frac{x^n}{[p(x)]^{1/2}} = \mathcal{H}_n(z_2, a, b, c) - \mathcal{H}_n(z_1, a, b, c).$$

Let $r_1 < r_2$ be the two roots of $p(x)$; r_1 and r_2 are real by virtue of condition (ii) above. The functions $H_n(r_1, r_2, a, b, c)$ then simplify to the functions $\bar{H}_n(a, b, c)$:

$$\bar{H}_0(a,b,c) = \pi/(-a)^{1/2},$$

$$\bar{H}_1(a,b,c) = (-b/2a)\,\bar{H}_0(a,b,c),$$

$$\bar{H}_2(a,b,c) = \left(\frac{3b^2 - 4ac}{8a^2}\right)\bar{H}_0(a,b,c),$$

$$\bar{H}_3(a,b,c) = -\left(\frac{5b^3}{16a^3} - \frac{3bc}{4a^2}\right)\bar{H}_0(a,b,c),$$

$$\bar{H}_4(a,b,c) = \left(\frac{35b^4}{128a^4} - \frac{30b^2c}{32a^3} + \frac{12c^2}{32a^2}\right)\bar{H}_0(a,b,c).$$

---

*Work supported by the Camille and Henry Dreyfus Foundation.

[1]For recent reviews see: (a) M. J. Cooper, Adv. Phys. 20, 453 (1971); (b) I. R. Epstein, Acc. Chem. Res. 6, 145 (1973); (c) I. R. Epstein, in *MTP International Review of Science*, edited by A. D. Buckingham (Butterworths, London, 1975), Vol. 12, p. 107; (d) B. G. Williams, *The Compton Effect* (McGraw-Hill, New York, to be published).

[3]B. G. Williams, *Standardization of Compton Profile Measurements—The Compton Profile of Water*, preliminary report, I. U. Cr. Commission on Charge, Spin and Momentum Density (University of Warwick, Coventry, U. K., 1974).

[4]B. G. Williams, P. Pattison, and M. Cooper, Philos. Mag. 30, 307 (1974).

[5]J. Felsteiner, P. Pattison, and M. Cooper, Philos. Mag. 30, 537 (1974).

[6]Paper I: A. C. Tanner and I. R. Epstein, Phys. Rev. A 13, 335 (1976).

[7]W. Lichtenberg and A. Przybylski, Nucl. Instrum. Methods 98, 99 (1972).

[8]V. Halonen, B. G. Williams, and T. Paakkari, Phys. Fennica (to be published).

[9]Paper III: A. C. Tanner and I. R. Epstein, following paper, Phys. Rev. A 14, 328 (1976).

[10]J. W. M. Dumond, Phys. Rev. 36, 1685 (1930).

[11]P. Kirkpatrick, Phys. Rev. 52, 1201 (1937).

[12]W. R. McIntire, Phys. Status Solidi A 23, 359 (1974).

[13]A. C. Tanner, thesis (Brandeis University, 1975) (unpublished).

[14]B. G. Williams and V. Halonen, Phys. Fennica 10, 5 (1975).

[15]We shall actually consider only cases for which $d\sigma/d\Omega$ is *independent* of φ.

[16]μ_c and μ_R: E. Storm and H. I. Israel, Los Alamos Scientific Laboratory publication LA-3753, Los Alamos, New Mexico, 1967 (unpublished). Our Compton attenuation coefficient μ_c corresponds to $\mu_{\mathrm{INC}}^{\mathrm{BD}}$ of Storm and Israel. μ_τ and μ: J. H. Hubbell, *Photon Cross Sections, Attenuation Coefficients, and Energy Absorption Coefficients From 10 keV to 100 GeV*, NSRDS-NBS N35, Circ. No. 29 (U. S. GPO, Washington, D. C., 1969).

[17]I. S. Gradshteyn and I. M. Ryzhik, *Tables of Integrals, Series, and Products* (Academic, New York, 1965).

[18]H. B. Dwight, *Tables of Integrals and Other Mathematical Data*, 4th ed., (MacMillan, New York, 1972).